Network Optimization of Functional Connectivity Within Default Mode Network Regions to Detect Cognitive Decline

W. Art Chaovalitwongse, *Senior Member, IEEE*, Daehan Won, *Member, IEEE*, Onur Seref, *Member, IEEE*, Paul Borghesani, M. Katie Askren, Sherry Willis, and Thomas J. Grabowski

***Abstract*— The rapid aging of the world's population is causing an increase in the prevalence of cognitive decline and degenerative brain disease in the elderly. Current diagnoses of amnestic and nonamnestic mild cognitive impairment, which may represent early stage Alzheimer's disease or related degenerative conditions, are based on clinical grounds. The recent emergence of advanced network analyses of functional magnetic resonance imaging (fMRI) data taken at cognitive rest has provided insight that declining functional connectivity of the default mode network (DMN) may be correlated with neurological disorders, and particularly prodromal Alzheimer's disease. The goal of this paper is to develop a network analysis technique using fMRI data to characterize transition stages from healthy brain aging to cognitive decline. Previous studies primarily focused on inter-nodal connectivity of the DMN and often assume functional homogeneity within each DMN region. In this paper, we develop a technique that focuses on identifying critical intra-nodal DMN connectivity by incorporating sparsity into connectivity modeling of the k-cardinality tree (KCT) problem. Most biological networks are efficient and formed by sparse connections, and the KCT can potentially reveal sparse connectivity patterns that are biologically informative. The KCT problem is NP-hard, and existing solution approaches are mostly heuristic. Mathematical formulations of the KCT problem in the literature are not compact and do not provide good solution bounds. This paper presents new KCT formulations and a fast heuristic approach to efficiently solve the KCT models for large DMN regions. The results in this paper demonstrate that traditional fMRI group analysis on DMN regions cannot detect any statistically significant connectivity differences between normal aging and cognitively impaired subjects in DMN regions, and the proposed KCT approaches are more sensitive than the state-of-the-art regional homogeneity approach in detecting significant differences in both left and right medial temporal regions of the DMN.**

***Index Terms*— Network, valid inequalities, fMRI, cognitive decline, biomarkers**

I. Introduction

DESPITE abundant evidence for cognitive decline as a feature of normal aging, there is wide variability in the extent and progression of these age-related changes [1]. Mild cognitive impairment (MCI) has been defined as an intermediate stage between normal age-related cognitive changes and dementia [2]. Current diagnosis of MCI is based on the patient or provider having an objective cognitive concern while their overall cognitive function remains intact. This often results in delayed detection and would hamper the dissemination and utility of neuroprotective treatments as they are developed in the future. Thus, there is a pressing need for quantitative neurophysiological methods that can be used to assess brain function before overt cognitive decline occurs. This study presents a step toward the development of a sensitive, non-invasive neuroimaging tool to detect abnormal brain function early, prior to overt cognitive change. We develop a novel network analysis technique to investigate if the strength and structure of brain connectivity within functional regions are altered and associated with cognitive decline.

Advances in functional magnetic resonance imaging (fMRI) have allowed researchers to define alterations in large scale neuronal networks that may be associated with abnormal cognitive changes. In one popular paradigm, fMRI data is acquired while an individual lies, resting, in the scanner (aka *resting state fMRI*) and major "intrinsic" brain networks are defined via correlations in low frequency (0.1-0.01 Hz) spontaneous fluctuations in the blood oxygen level-dependent (BOLD) signal. Intrinsic networks identified in resting state fMRI show close correspondence to those found in task-related functional

Manuscript received May 15, 2016; revised November 6, 2016; accepted January 28, 2017. This work was supported in part by the National Science Foundation grant CMMI under Grant 1333841 and in part by the National Institutes of Health under Grant RC4-NS073008-01 and Grant R37-AG024102-10.

W. A. Chaovalitwongse is with the Institute for Advanced Data Analytics and the Department of Industrial Engineering, University of Arkansas, Fayetteville, AR 72701 USA (e-mail: artchao@uark.edu).

D. Won is with the Department of Systems Science and Industrial Engineering, Binghamton University, The State University of New York, Binghamton, NY 13902 USA (e-mail: dhwon@binghamton.edu).

O. Seref is with the Department of Business Information Technology, Virginia Polytechnic Institute and State University, Blacksburg, VA 24061 USA (e-mail: seref@vt.edu).

M. K. Askren is with the Integrated Brain Imaging Center and the Department of Radiology, University of Washington, Seattle, WA 98195 USA (e-mail: askren@uw.edu).

P. Borghesani and S. Willis are with the Department of Psychiatry and Behavioral Sciences, University of Washington, Seattle, WA 98195 USA (e-mail: paulrb@uw.edu; oldage@uw.edu).

T. J. Grabowski is with the Integrated Brain Imaging Center and the Departments of Radiology and Neurology, University of Washington, Seattle, WA 98195 USA (e-mail: tjgrabow@uw.edu).

Digital Object Identifier 10.1109/TNSRE.2017.2679056

imaging experiments supporting their functional significance during cognition [3]. Default mode network (DMN), which includes multiple spatially distinct regions in all lobes of the cortex [4], [5], is among the major intrinsic networks defined via this method. Alterations of functional connectivity in the DMN have been shown to be associated with neurological disorders such as dementia [6], schizophrenia [7], autism spectrum disorder [8], and depression [9]. However, most conventional fMRI studies of the DMN focus on examining *coarse functional connectivity* between spatially distinct DMN regions, called **inter-regional connectivity**, by simply averaging fMRI signals within DMN regions and measuring correlation strengths as large-scale connectivity between the regions. This approach simply assumes the homogeneity of fMRI signals within individual DMN regions and overlooks the importance of connectivity between fMRI signals in the same region, called **intra-regional connectivity**. Although there has been some evidence of disrupted inter-regional connectivity among DMN regions in neurodegenerative diseases, the role of intra-regional connectivity that might be associated with the diseases is still largely unknown. For instance, alterations in inter-regional connectivity structure among the DMN regions were found in Alzheimer's disease (AD); however, intact prefrontal and temporal networks were still found in both elderly controls and AD patients [10]. Thus investigation of intra-regional connectivity is worthwhile and can be complementary to the existing inter-regional connectivity studies in the literature. The regional homogeneity approach (ReHo) is thought to be the current state-of-the-art method in measuring similarity of BOLD time series of a given voxel to those of its nearest neighbors in a voxel-wise way [11]. However, it does not take into account of patterns (e.g., path or hub-and-spoke) of intra-regional connectivity.

Although the DMN regions are commonly defined within the entire study subject group (for an "unbiased" comparison), the actual functional regions for individual subjects can almost certainly vary in size, shape and exact location. This makes investigation of intra-regional connectivity with variable DMN regions very challenging. For example, Figure 1 illustrates the DMN regions defined by group analysis (n=29 subjects) and compares the locations, sizes and shapes of DMN regions constructed by the group DMN regions on 3 individual subjects. The figure shows that larger regions (e.g., the right dorsal parietal region of the DMN) are highly variable between subjects (top row). To address this challenge, we propose a network optimization approach to characterize the strength and structure of intra-regional connectivity by using a spanning tree model. In network optimization, the most commonly used spanning tree model is the minimum spanning tree (MST). The MST has been used in a study of childhood-onset Schizophrenia [12] to investigate inter-regional functional connectivity but has not been used to explore intra-regional connectivity. Because the MST makes the unsubstantiated assumption that every voxel has to be connected, the MST might not be robust enough for intra-regional connectivity analysis as DMN regions are not precisely defined and vary in size and location across subjects. We propose the k-cardinality tree (KCT) model with varying numbers of k voxels to be connected

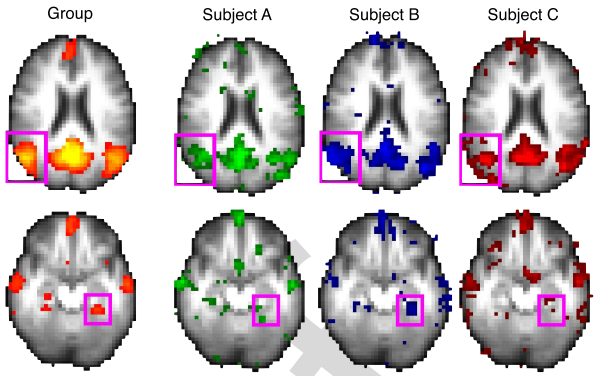

Fig. 1. Variability in DMN regions identified by dual regression. Top row illustrates variability in large regions (pink box - right dorsal parietal) while the bottom row shows the extreme heterogeneity of smaller regions (pink box - left posterior hippocampus). Group results from 29 subjects.

within each DMN region to investigate the robustness and stability of intra-regional functional connectivity by taking into account the functional heterogeneity within individual DMN regions. Specifically, the KCT model can identify the connected voxels with varying sizes of the critical component within individual DMN regions, and in turn investigate different locations and sizes of functional connectivity within DMN regions. In contrast to the standard MST, the KCT is NP-hard and very difficult to solve. Existing KCT formulations in the literature are not scalable and do not provide good solution bounds. We develop new compact mathematical programming models, which provide better linear programming relaxation bound than existing models, and a new algorithm to efficiently solve large-scale KCT models for large DMN regions. Using the proposed KCT approach, we investigate alterations of functional connectivity in the DMN and other cognitive-related networks in a cross-sectional sample of aging individuals with normal aging and abnormal cognitive decline. The outcome of this study might result in a non-invasive technique that could be used as a diagnostic tool that is sensitive enough to detect alterations in functional networks for early detection of MCI.

The remainder of the paper is organized as follows. In Section 2, we give a brief background on current MCI and AD studies, fMRI analyses and KCT solution approaches. In Section 3, we provide detailed information on the dataset used in this study, fMRI data pre-processing, and statistical analyses to identify the DMN regions. In Section 4, we present mathematical formulations for the KCT problem and a scalable, fast heuristic method. In Section 5, we present the computational results, analyses of our findings and the outcome from a population-based comparison. We provide conclusions and final remarks in the final section of this paper.

II. Background

A. Resting State fMRI and Default Mode Network (DMN)

In resting state fMRI, subjects are asked to rest, calmly and comfortably, in the scanner and data is collected over 5-10 minutes. Spatial correlations of low frequency oscillations in the BOLD signal can then be used to map large scale

neural systems in the brain, i.e., functional connectivity [13]. Resting state fMRI has allowed neuroscientists to discover the organization and connectivity of large-scale intrinsic connectivity networks (ICNs). Functional interactions within and between these ICNs provide unique information about systems-level brain function not obtainable through conventional task-based fMRI and most other neuroimaging methods. The DMN is the prototypical ICN. The DMN can be subdivided into multiple regions that have correlated low frequency BOLD signals and whose overall activity and synchrony is related to ongoing cognitive states. Identifying the functional area of each DMN region can be challenging. There are four typical methods used to define DMN regions (reviewed in [14]). First, seed-voxel (or region) based approaches can be employed to determine where fMRI signal is correlated with a specific voxel (or region). A fundamental problem with this method is that a standard space seed voxel may not fall in the same region across subjects and/or the resultant intra-regional connectivity map may not represent the same network across subjects. Second, fMRI data can be analyzed with independent component analysis (ICA) that, with no a priori guidance, decomposes data into individual spatial components. However, components (i.e., regions and networks) identified in single subjects are highly variable and difficult to compare across subjects. Group ICA (e.g., dual regression) allows for the identification of common components, but the presence of these regions and networks in individual subjects is not ensured. Third, DMN regions may be defined by their correlated activity during a cognitive task (aka activation map). This univariate analysis allows for the assumption that the region is involved with a higher cognitive function but does not necessary mean that the regions are "working together" [15]. In addition, regions taken from a group activation map may not represent the true location of the region in an individual. Fourth, anatomical constraints can be used to define DMN regions by dividing (parcellating) the cortex into varying numbers of regions. Although these standardized parcellation methods may be applied across studies, they introduce significant errors given that cortical areas that represent functional regions (and hence the topology of local regions) likely vary across subjects.

B. Alterations of DMN in Aging

Higher cognitive abilities (memory, executive function, etc.) emerge from complex activity of distributed cortical regions, each variably specialized for one or more aspects of the cognitive process. Research suggests that cognitive decline, both age-related and pathological, may result from dysregulation of these large scale networks and that these changes can be mapped using resting state fMRI [16]. Several studies have demonstrated a relationship between the connectivity strength and/or the activity within DMN and cognitive decline [4], [17], [18], and overall, large-scale connectivity is thought to decline in older individuals [19], [20]. Graph theoretic approaches have found reduced centrality, or importance, of frontal networks with increased centrality of the DMN in aging [21] although there are reports of decreased inter-regional DMN connectivity being associated with cognitive decline [18]. These divergent findings justify our investigation of the association between DMN and cognitive decline in both normal and abnormal aging. Although changes in overall DMN behavior would result in corresponding changes in brain connectivity, especially associated with aging [22], functional connectivity within DMN regions may provide a more complete picture of fine-level dynamics and age-related changes. Our study focuses on a network analysis that incorporates intra-regional data into functional connectivity quantification of the DMN rather than limiting ourselves to a global "network" across DMN regions.

C. K-Cardinality Tree (KCT) Problem

Given a connected undirected graph with a cost function defined on edges and a positive integer k, the KCT problem is to find a minimal cost tree of a graph with exactly k edges. The KCT formulation was first introduced in [23], where it was proved to be NP-hard when $2 \leq k \leq |V| - 2$, where V is the number of vertices. The first integer programming formulation of the KCT problem based on general subtour elimination constraints (GSEC) was proposed in [23]. Because there are an exponential number of constraints in terms of the graph size, a branch-and-cut algorithm to solve the GSEC formulation was later developed in [24]. However, the algorithm was inefficient and only able to solve the instances up to 30 nodes. In the literature, solution approaches of the KCT problem are mostly heuristic and metaheuristic approaches [25]–[29]. There have been a few studies on approximation algorithms for the KCT problem [30]–[33] and many are based on the primal & dual analysis that was motived by the prize-collecting Steiner tree problem [34]. Although some of these methods provided a reasonable solution time, they are quite hard to implement and not generalizable. In addition to metaheuristic approaches mentioned previously, over the past ten years there have been only four main exact solution approaches based on mixed-integer programming (MIP). First, two branch-and-bound approaches were proposed to solve two KCT formulations, one using multi-commodity flow (MCF) constraints to enforce connectivity of the resulting tree and cycle prevention and another using the Miller-Tucker-Zemlin (MTZ) constraints [35]. The study also expanded the formulation and applied a Lagrangian relaxation method, which could be embedded into a branch-and-bound procedure. Second, the GSEC reformulation was proposed in [36] based on generalized cut set inequalities to eliminate subtours, and a new branch-and-cut approach was employed to solve the KCT problem. In addition, because the formulation is defined over a digraph, they also proposed asymmetry constraints to exclude symmetric solutions. Third, [37] proposed the rooted version of KCT (RKCT), where a node to be included in the KCT solution is pre-determined. This approach solves the KCT problem sequentially by selecting a different root node in each iteration until all possible root nodes are considered. In the most recent study, [38] presented a more advanced version of the branch-and-cut approach proposed in [36]. Three new families of valid inequalities were introduced, and two of them were facet

defining inequalities for the polytope defined by the convex hull of feasible KCT solutions. The approach was shown to outperform all other approaches that have been developed, especially for grid-graph instances. It is also worth noting that all of the approaches mentioned above, except RKCT, were applied to the KCT reformulation defined over digraphs. Digraphs can be constructed by introducing two edges with the same end nodes and the opposite directions for every edge in the original graph, and adding one or more artificial nodes. Therefore, feasible solutions to the reformulation imply spanning arborescences for its digraph. Note that the above-mentioned approaches appear to work well on grid graphs, which are sparse. Because intra-nodal connectivity networks from fMRI data result in a very dense graph, existing KCT approaches are not efficient enough to solve networks of this size, and this motivates the methodological development in this paper.

III. Functional Connectivity of fMRI Data

A. Data Set

The Seattle Longitudinal Study (SLS) is a cohort-sequential longitudinal study that began in 1956 with cognitive and behavioral assessment of all available prior participants and a new random sample occurring every 7-years. Cognitive measures include an extensive battery of tests to examine memory, executive function, perceptual speed, and psychomotor speed. The total number of subjects in the SLS is 6,000, and there are currently $3,000$ active participants. From these active subjects, $>$ 200 individuals for whom midlife cognitive data spanning $>$ 3 assessments (i.e., 14 years) were selected for a longitudinal neuroimaging study of midlife cognitive change and risk of cognitive decline. Midlife cognitive data in three domains (episodic memory, executive function, psychomotor speed) was examined for each participant and they were categorized as declining or stable in each domain. The data set used in this study include 29 typically aging subjects for who $>$ 10 years of longitudinal cognitive testing data were available. These subjects were selected from the Seattle Longitudinal Study [39] to undergo structural MRI, and functional imaging (resting state fMRI and task-associated fMRI). This paper is focused on the functional connectivity analysis of the resting state fMRI, which consists of 7.5-minutes of BOLD-fMRI data collected while subjects lay comfortably with their eyes open in the scanner (TR = 2 seconds). During midlife (defined as age 44-64), the 29 subjects were classified a priori as having declining ($n = 11$) or stable ($n = 18$) executive function based on word fluency, abstract reasoning and cognitive flexibility. Demographic, neuroimaging and executive function characteristics of the subjects are provided in Table I. Note that although the decliners had declined earlier than (stable) non-decliners as well as had been at risk for progression to MCI, both decliners and non-decliners were not MCI at the time of scan when the subject data were collected.

TABLE I
Characteristics of Subjects in Decliner and Stable Groups

	Decline	Stable (Non-Decliner)
N (male)	11 (3)	18 (9)
age (s.d.)	60 ± 3	60 ± 3
#APOE e4+ (total#)	4 (10)	7 (14)
Brain volume ± s.d.	1396 ± 85	1411 ± 66
WMH volume ± s.d.	32 ± 34	84 ± 135
Reasoning ± s.d.	53.0 ± 6.6	62.3 ± 6.5
Word fluency ± s.d.	52.2 ± 4.9	57.2 ± 8.4
Cognitive flexibility ± s.d.	54.4 ± 3.9	59.1 ± 3.8
Composite cExF ± s.d.	53.2 ± 3.7	59.5 ± 5.2
Composite delta ExF ± s.d.	-5.1 ± 2.0	3.3 ± 2.3

B. Data Pre-Processing

At the individual level, resting state fMRI data were pre-processed using standard methods in FEAT (FMRI Expert Analysis Tool) Version 5.98, part of FSL (Functional MRI of the Brain (FMRIB) Software Library, www.fmrib.ox.ac.uk/fsl). Data pre-processing steps we employed to remove non-neuronal sources of variance are as follows: non-brain removal with the Brain Extraction Tool; motion correction with MCFLIRT; spatial smoothing using a 6 mm full-width half-maximum (FWHM) Gaussian kernel; high-pass temporal filtering; bias-correction and grand-mean intensity normalization of the entire 4D dataset; 3D despiking (afni.nimh.nih.gov), removal of confounding signals (linear drift) through regression (white matter/CSF signal intensity time course, motion parameters, and noise components estimated using ICA). Subjects' fMRI data were registered to their high-resolution structural scans by using a boundary-based registration procedure. No subjects had excessive head motion during the scan; therefore, we did not exclude any subjects in this analysis.

C. Data Analysis

After fMRI data were preprocessed, the next step of our analysis was to isolate group and subject specific regions of the DMN. After DMN regions for individual subjects were obtained, we used the fMRI BOLD time series of all voxels within each region to calculate an all pairwise correlation coefficient matrix to construct a functional connectivity graph, which was used as input of our KCT models.

1) Identifying DMN Regions: Traditionally DMN regions have been defined either anatomically, using either standardized cortical maps [40] or individually defined regions, or functionally, by independent component analysis (ICA) methods [41]. Although an anatomical scheme is quite powerful, it raises potential confounds such as an arbitrary choice of threshold value applied to systematic sparsity differences and the incorrect assumption that regions would be of similar size and in precise enough cortical location across individuals. To robustly identify DMN regions, we employed a commonly used group ICA dual regression method [42] to the entire subject population (both cognitive declining and stable subjects). The process can be described as follows. First, we performed group ICA analysis by (1) mapping fMRI data of individual subjects in the population ($n = 29$) into a standard space, (2) concatenating fMRI BOLD time series of individual subjects and (3) subsequently running ICA analysis. The components (regions) of the DMN were identified by visual inspection of the group ICA results by pattern-matching

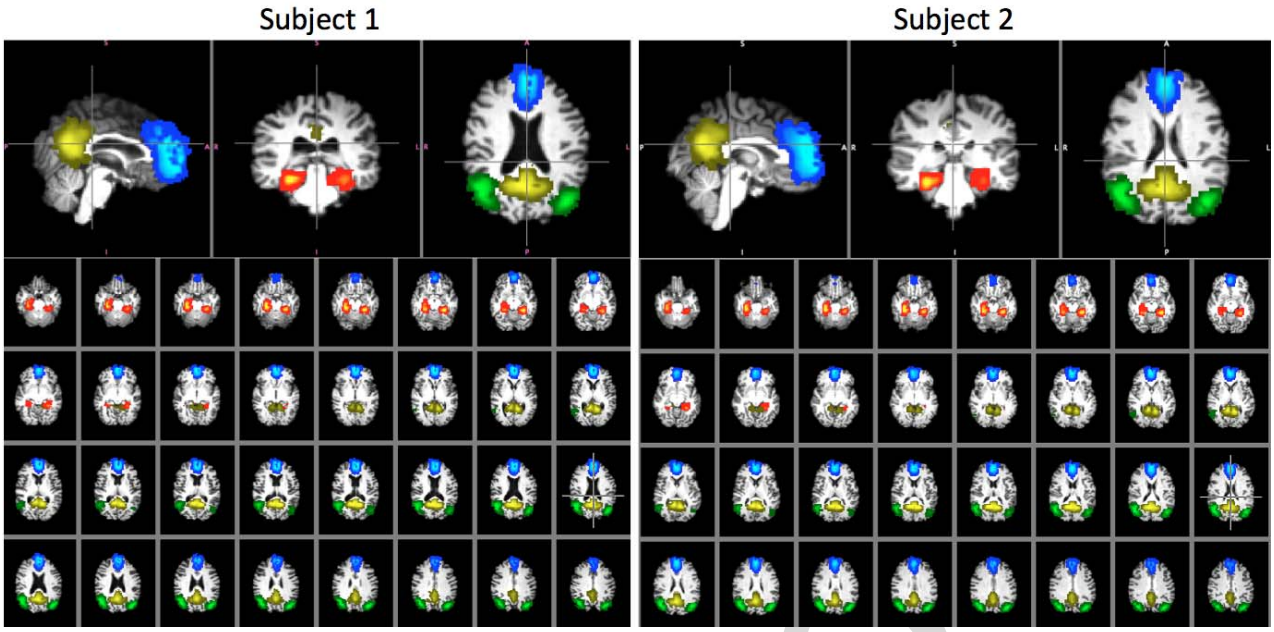

Fig. 2. DMN regions identified by dual regression from 29 subjects that are warped into two individual subjects' brains. Top row illustrates three different views of the DMN local regions of the two subjects: Sagittal View, Coronal View and Axial View, respectively. Bottom row shows the slice views of the DMN local regions: MFC region (blue), PCC region (yellow), and the right and left DPC (green), and MTL (red).

TABLE II
THE RANGE, AVERAGE AND STANDARD DEVIATION OF THE NUMBERS OF VOXELS (N) IN DIFFERENT DMN REGIONS ACROSS SUBJECTS

Statistics	DMN Regions					
	MFC	PCC	lLPC	lMTL	rLPC	rMTL
Range [Min–Max]	[719–1062]	[538–929]	[222–317]	[93–128]	[310–479]	[110–189]
Average ± std	878 ± 83	716 ± 94	271 ± 25	109 ± 9	401 ± 38	147 ± 18

ICA components with typical DMN regions. Subsequently, the average fMRI BOLD signal of each identified ICA component was calculated for each subject and then used (in separate individual regression) to generate a new, subject specific map of the DMN regions. In this study, we selected the following 6 local regions of the DMN, as shown in Figure 2:

- Region 1: (Bilateral) Medial Frontal Cortex (MFC),
- Region 2: (Bilateral) Posterior Cingulate Cortex (PCC),
- Region 3: Left Dorsal Parietal Cortex (lDPC),
- Region 4: Left Medial Temporal Lobe (lMTL),
- Region 5: Right Dorsal Parietal Cortex (rDPC),
- Region 6: Right Medial Temporal Lobe (rMTL).

It is worth noting that there is no ground truth of the accurate DMN location for each individual subject. Based on the most commonly used DMN identification method, we found that a traditional group comparison of connectivity differences between groups yielded no significant difference among these 6 DMN regions between cognitive declining and stable subjects. Because the DMN regions are defined in the standard MNI space, to perform analysis at the subject level the mask of each region is transformed to the subject space. This results in different number of voxels across different subjects. For each of the six DMN regions, Table II shows the range, average and standard deviation of the number of voxels (rounded to the nearest integer) in the subject space across all subjects. We note that the size of the KCT problem is defined by the number of voxels included in the region.

2) Constructing Local Connectivity Graphs: After DMN regions were defined, a local connectivity graph was created for each DMN region based on the functional connectivity matrix of all voxel pairs within the region. Specifically, the connectivity matrix was constructed by calculating absolute correlation coefficients between all pair-wise fMRI BOLD time series of all voxels in the region. The local connectivity graph is thus represented by a symmetric $N \times N$ functional connectivity matrix of all voxel pairs, where N is the number of voxels in the DMN region. Each entry of the matrix is associated with a voxel, and represents an absolute correlation coefficient between the voxel and another voxel in the DMN region. The greater the entry value, the higher connectivity. Note that the connectivity graph, which is the input into our KCT approaches, is a full graph, in which there exists an edge between every voxel (node) pair. From a neuroscientific stand point, our graph is not anatomically constrained because, due to a fissure (sulcus) on the surface of the brain, adjacent voxels may be associated with different cortical fields.

IV. EXACT AND HEURISTIC KCT APPROACHES

The KCT model for characterizing intra-regional functional connectivity can be mathematically modeled as follows. Let $G = (V, E)$ be a connected undirected graph with a set of vertices V, each representing a fMRI voxel within a DMN region, and a set of edges E, each representing a pair-wise connectivity between voxel pairs within the DMN region. The pair-wise connectivity cost of an edge is herein defined by the z-score of the correlation coefficient between BOLD time series of the two voxels connected by the edge. The positive integer k is a parameter to control the size of the functional connectivity tree, which in turn controls the number of selected voxels in the DMN region. Traditional KCT problem is to find a minimum cost tree with exactly k edges. In this paper, our

KCT problem is to find the maximum cost tree as to construct the most highly connected voxels as a tree of size k within each DMN region, which can be transformed to a traditional KCT problem by multiplying the z-scores by -1.

In this paper, we present two new mixed integer programming (MIP) formulations for the KCT problem. The main building blocks of our formulations are connectivity constraints and combinatorial constraints, which include cardinality and degree constraints. The connectivity constraints are based on single commodity flow and cycle elimination to define a tree solution. The first formulation is called "single flow" model, which is much more compact as it uses a smaller number of flow variables compared to an existing multi-commodity flow formulation [35]. The second formulation, called "modified MTZ" model, uses node selector variables and provides a better LP relaxation bound than the MTZ model in the literature. We also introduce symmetry breaking constraints that can eliminate symmetrical solutions for the MIP formulations and speed up the computational efficiency of our model. Finally, we introduce a greedy algorithm to efficiently solve large-scale KCT problems.

A. Structure and Cardinality: Connectivity Constraints

Given an undirected graph $G = (V, E)$, an edge $e \in E$ is defined as $\{i, j\}$ with endpoints of vertex i and j. For a given directed graph $D = (V, A)$, we denote an arc $a \in A$ whose start vertex is i and end vertex j by (i, j). For a subset of vertices $S \subset A$, we define the arc sets, $\delta^+(S) = \{(i, j) \in A | i \in S, j \notin S\}$, as the set of outgoing arcs for S, and $\delta^-(S) = \{(i, j) \in A | i \notin S, j \in S\}$, as the set of incoming arcs for S. We use the notation $\delta^+(i)$ and $\delta^-(i)$ if S has a single vertex.

We introduce our KCT formulations on a directed graph, therefore we transform KCT problem in an undirected graph $G = (V, E)$ to a KCT problem in a directed graph $D = (V, A)$ by replacing each edge $\{i, j\} \in E$ with arcs (i, j) and (j, i) with the same cost as the edge, i.e. $c_{(i,j)} = c_{(j,i)} = c_{\{i,j\}}$. Following a similar construction as in [36], we further consider augmenting D into $\hat{D} = (\hat{V}, \hat{A})$ by introducing an artificial root vertex with index 0 and additional arcs $(0, i)$ for all $i \in V$ with zero cost, such that $\hat{V} = V \cup \{0\}$, and $\hat{A} = A \cup \{(0, i)\ \forall i \in A\}$. This root vertex along with any immediate arc are to be removed from the solution to reveal the solution to the KCT problem.

We define $x_a \in \{0, 1\}$ to be arc selector variables and $y_i \in \{0, 1\}$ to be vertex selector variables. We build our KCT formulations incrementally to demonstrate the functionality of different sets of constraints. We start with the following combinatorial set that defines the combinatorial structure of the feasible solutions.

$$S_{CC}: \sum_{a \in A} x_a = k, \tag{1a}$$

$$\sum_{i \in V} y_i = k + 1, \tag{1b}$$

$$\sum_{a \in \delta^-(i)} x_a + x_{(0,i)} = y_i \quad \forall\, i \in V, \tag{1c}$$

$$\sum_{a \in \delta^+(0)} x_a = 1, \tag{1d}$$

$$x_{(i,j)} + x_{(j,i)} \leq y_i \quad \forall\, (i, j) \in A, \tag{1e}$$

$$x_a, y_i \in \{0, 1\}, \quad \forall\, i \in V, \quad \forall a \in A. \tag{1f}$$

Constraints (1a) and (1b) require that exactly k arcs and $k + 1$ vertices must be selected from the original network. Constraints (1c) require that a selected vertex can have only one selected incoming arc, and none otherwise. Constraint (1d) enforces that only one outgoing arc from the artificial root vertex 0, which is used to determine the actual root of the arborescence. Constraints (1e) require that either arc (i, j) or its reverse arc (j, i) should be selected if vertex i exists, and neither otherwise.

Proposition 1: Each solution in S_{CC} is composed of connected components with at most one cycle.

Proof: Note that due to the constraint (1e), two-vertex cycles are not possible in S_{CC}. Due to the constraints (1d), which imply that every vertex can have only one parent vertex (except for vertex 0), one can start with any arbitrary vertex and trace back to a root vertex or itself within a connected component. Let C denote a connected component in a solution that satisfies S_{CC}. Assume that there are two cycles $W_1 \in C$ and $W_2 \in C$. Let $W_1 \cap W_2 \neq \emptyset$; then there is at least one vertex in $W_1 \cap W_2$, whose in-degree is 2. Thus, it contradicts constraints (1d). Let $W_1 \cap W_2 = \emptyset$; then there is a directed path between W_1 and W_2, which means that a vertex in W_1 or W_2 has in-degree of 2, which again contradicts (1d). ■

Proposition 1 implies that the connected components in S_{CC} are either directed trees or they contain a single cycle that can be broken to construct an arborescence, which may facilitate finding KCTP solutions after inserting connectivity and subtour elimination constraints.

B. Cycle Prevention Constraints

We introduce two sets of cycle prevention constraints to be integrated with the connectivity constraints introduced in the previous section. This results in two alternative MIP formulations to solve the KCT problem.

1) Single Commodity Flow (SCF) Constraints: One possible way of assuring connectivity is to create a flow from the root vertex to all of the other vertices via selected arcs, which can be incorporated into our model by flow conservation constraints. Such constraints would establish connections between separate connected components of a solution in S_{CC} and the cardinality constraint (1a) would prevent cycles, thus creating a tree structure with k arcs. Let variable f_a denote a flow value on arc a, $x_a \in \{0, 1\}$ denote the arc selector variables, and $y_i \in \{0, 1\}$ denote the vertex selector variables. Then the following constraints establish connectivity through conservation of flow:

$$S_{SCF}: \sum_{a \in \delta^+(i)} f_a \leq k\, y_i, \quad \forall i \in V, \tag{2a}$$

$$\sum_{a \in \delta^-(i)} f_a - \sum_{a \in \delta^+(i)} f_a = y_i, i \in V, \tag{2b}$$

$$f_a = (k + 1)x_a \quad \forall a \in \delta^+(0) \tag{2c}$$

$$f_a \leq k x_a, \quad \forall a \in A. \tag{2d}$$

Constraints (2a) require that at most k units of flow can leave a vertex if it is in the tree, and none otherwise. Constraints (2b) ensure that one unit of flow is consumed by each vertex in the

tree and constraints (2c) requires that the selected artificial arcs from vertex 0 will move $k+1$ units of flow to be distributed to the tree. Constraints (2d) require that at most k units of flow is permitted to flow on an arc a. Combining the properties of sets S_{CC} and S_{SCF}, we introduce a new single commodity flow formulation Eq. (3) to solve the KCT problem.

$$P_{SCF} : \min_{x,y,f} \left\{ \sum_{a \in A} c_a x_a : (x, y, f) \in S_{CC} \cap S_{SFC} \right\} \quad (3)$$

2) Miller-Tucker-Zemlin (MTZ) Constraints: MTZ constraints are proposed to eliminate subtours in the traveling salesman problem [43], which involve continuous variables that represent the depth of a vertex with respect to a root vertex. MTZ constraints can be lifted to produce tighter bounds as shown in [44], which are used to solve the KCT problem [35]. Let u_i, $i \in V$ denote the depth variables, $x_a \in \{0, 1\}$ denote the arc selector variables, and $y_i \in \{0, 1\}$ denote the vertex selector variables. Then, we incorporate the following lifted MTZ constraints to eliminate the cycles that may exist in the solutions of S_{CC}.

$$S_{MTZ} : u_i \leq k y_i \quad \forall i \in V, \quad (4a)$$

$$(k+1)x_{(i,j)} + (k-1)x_{(j,i)} + u_i - u_j \leq k \quad \forall (i, j) \in A, \quad (4b)$$

$$(k+1)x_{(0,j)} - u_j \leq k \quad \forall (0, j) \in \hat{A} \quad (4c)$$

Constraints (4a) require that the depth of a vertex can at most be k. Constraints (4b) are MTZ constraints for the regular arcs in the network, and constraints (4c) are MTZ constraints for the additional arcs leaving the artificial root vertex 0 in the augmented network. Combining the properties of sets S_{CC} and S_{SCF}, we introduce the MTZ based formulation in Eq. (5) to solve the KCT problem.

$$P_{MTZ} : \min_{x,y,u} \left\{ \sum_{a \in A} c_a x_a : (x, y, u) \in S_{CC} \cap S_{MTZ} \right\} \quad (5)$$

C. Symmetry Breaking Constraints

One drawback that is common to all of the above formulations that use directed graphs is the problem of symmetric solutions. In other words, there are $k+1$ equivalent solutions, each starting with one of the $k+1$ vertices as the root of the tree. A symmetry breaking constraint proposed by [38] significantly reduces the search tree in branch-and-bound or branch-and-cut type algorithms. It can be adapted to formulations P_{SCF} and P_{MTZ} by including the following constraints,

$$\sum_{j>i} x_{(0,j)} + y_i \leq 1, \quad \forall i \in V. \quad (6)$$

Let vertex j^*, where $x_{(0,j^*)=1}$, be denoted as the actual root of the solution tree. Then, constraints (6) force the condition $\sum_{j>i} x_{(0,j)} = 0$ for any vertex i, where $y_i = 1$. This means that vertices with indices larger than i cannot be the actual root in the solution, which implies that the index of the actual root has to be smaller than the indices of the other tree vertices to break the symmetry.

Input: $D = (V, A)$
Output: T^*
$\mathcal{I} \leftarrow SortedArcIndex(c(A))$
$\mathcal{T}(i) \leftarrow i \ \forall i \in V$
$deg(i) \leftarrow 0 \ \forall i \in V$
$i \leftarrow 0, T \leftarrow \emptyset, t_{max} \leftarrow 0$
while TRUE **do**
  $i \leftarrow i + 1$
  $a \leftarrow A(\mathcal{I}_i)$
  if $\mathcal{T}(t(a)) \neq \mathcal{T}(h(a))$ **then**
    $T \leftarrow T \cup a$
    $\mathcal{T}(j) \leftarrow \mathcal{T}(t(a)) \ \forall j : \mathcal{T}(j) = \mathcal{T}(h(a)$
    $deg(t(a)) \leftarrow deg(t(a)) + 1$
    $deg(h(a)) \leftarrow deg(h(a)) + 1$
    $\mathcal{T}_{curr} \leftarrow \{j : \mathcal{T}(j) = \mathcal{T}(t(a))\}$
    if $|\mathcal{T}_{curr}| > t_{max}$ **then**
      $t_{max} \leftarrow |\mathcal{T}_{curr}|$
      if $t_{max} > k$ **then**
        break
      end if
    end if
  end if
end while
$T^* \leftarrow \{a \in T : t(a) \cup h(a) \in \mathcal{T}_{curr}\}$
while $|T^*| > k$ **do**
  $a^* \leftarrow \arg\max\{a \in T^* : deg(t(a)) = 1 \vee deg(h(a)) = 1\}$
  $T^* \leftarrow T^* \setminus a^*$
  $deg(t(a^*) = deg(t(a^*)) - 1$
  $deg(h(a^*) = deg(h(a^*)) - 1$
end while

Fig. 3. KCT-Kruskal: Greedy Algorithm.

D. Greedy Algorithm

To solve large instances of the KCT problem, which is NP-hard [23], we introduce a greedy algorithm, as shown in Fig. 3, to find a KCT solution based on Kruskal's algorithm for finding minimal spanning trees. Generally, Kruskal's algorithm grows a forest by adding connections in increasing order of their costs. Starting with each vertex being a separate tree, in each iteration two trees merge together, until there is one spanning tree. As the trees formed by Kruskal's algorithm in earlier iterations tend to have smaller costs due to the inclusion of arcs in ascending order of their costs, our algorithm keeps track of these low cost trees, and as soon as one of the trees have k or larger arcs we stop the execution of Kruskal's algorithm. Then, we iteratively remove the leaf arc with the largest cost from this tree until the component has exactly k arcs. In the algorithm, we denote the cost of all arcs with $c(A)$. We assume that subroutine $SortedArcIndex(c(A))$ returns the ordered indices $\mathcal{I}$ of arcs sorted in ascending order of their costs, where $\mathcal{I}_i$ refers to the i^{th} index. We use $A(k)$ to refer to arc with index k. We denote the tree label of vertex i in a forest of trees with $\mathcal{T}(i)$ and the degree of vertex i with $deg(i)$. We denote the set of arcs selected during the execution of Kruskal's algorithm T, the set of vertices in the most recent tree updated $\mathcal{T}_{curr}$ and the maximum tree size in the forest in terms of number of vertices as t_{max}. Finally, we refer to the set of arcs in the solution tree to be returned as T^*. The time complexity of the KCT-Kruskal heuristic algorithm is given in the following proposition.

Proposition 2: KCT-Kruskal runs in $O(|A| \log |A|)$ time.

Proof: Kruskal's algorithm is known to run in $O(|A| \log |A|)$ time complexity. Updating vertex degrees and removing the largest cost leaf arc can be done in constant time using simple data structures, thus reduction of the tree to

TABLE III
NUMBERS OF NON-FEASIBLE/SUB-OPTIMAL INSTANCES (OUT OF 29 INSTANCES) FOR EACH MIP MODEL

ROI	K = 10%				K = 25%			
	MTZ	MTZ*	SCF	MCF	MTZ	MTZ*	SCF	MCF
MFC	0/28	7/22	29/0	29/0	0/27	22/6	29/0	29/0
PCC	0/26	5/24	18/11	29/0	1/20	18/10	29/0	29/0
lLPC	0/0	0/6	0/0	10/19	0/0	0/11	0/2	27/2
lMTL	0/0	0/0	0/0	8/21	0/2	0/1	0/0	1/21
rLPC	0/1	0/8	0/0	12/17	3/0	3/12	0/17	29/0
rMTL	0/0	0/0	0/0	11/18	0/0	0/1	0/0	10/19
ROI	K = 50%				K = 75%			
	MTZ	MTZ*	SCF	MCF	MTZ	MTZ*	SCF	MCF
MFC	27/2	23/6	29/0	29/0	29/0	27/2	29/0	29/0
PCC	22/3	9/20	29/0	29/0	27/0	20/9	28/1	29/0
lLPC	1/1	0/23	0/6	29/0	0/0	0/29	0/7	29/0
lMTL	0/0	0/3	0/0	17/12	0/0	0/5	0/0	19/10
rLPC	9/4	5/24	3/22	29/0	4/2	11/18	3/24	29/0
rMTL	0/0	0/9	0/0	2/27	0/0	0/12	0/0	5/24

appropriate size takes $O(|A|)$ time. The overall complexity of the KCT-Kruskal algorithm is then $O(|A| \log |A|)$. ■

V. COMPUTATIONAL RESULTS

In this section, we present the computational results of our proposed models and heuristic approach on the fMRI data. All problems are solved using a Dell Precision T7600 workstation with two 2.0Ghz CPUs and 24 GB memory on a 64-bit Windows 7 platform. For the DMN analysis, the mathematical modeling is implemented in C♯ language using CPLEX callable library version 12.5. For every test instance, computation time limit was set to 1 hour (3,600 seconds). The heuristic approach was implemented in Matlab version 2012b. Because there are different numbers of voxels in the same DMN region across subjects, we used parameter "K" as a percentage of the number of voxels to be included from the total number of voxels in the region. We fixed the value of K to 10%, 25%, 50%, 75%. Note that when $K = 100\%$, the KCT problem is equivalent to the minimum spanning tree (MST) problem, which can be solved efficiently by standard MST approaches.

A. Computational Efficiency

In this subsection, we first report an account of solution status of the 29 instances over each region, followed by solution times (with 1 hour run time limit) for four different MIP models and the heuristic method. We used the MTZ and SCF models with symmetry breaking constraints, the MCF model proposed by [35], and the MTZ model without symmetry breaking constraints (denoted by MTZ*). Table III shows the solution status of MIP models for each region and $K\%$ as the count of *non-feasible/sub-optimal*. For example, for PCC region at $K = 50\%$, out of 29 instances the MTZ model found a sub-optimal solution in 3 instances, achieved optimality in 4 instances, and was not able to find a feasible solution in 22 instances. From the table, we observe that the MCF model performed very poorly as it did not reach optimality in any region and $K\%$ combination. Thus we shall eliminate it from the remainder of the computational results. In the larger instances such as MFC and PCC regions with more than 500 nodes, we observe that optimality was rarely achieved by the MTZ and MTZ* models, and never achieved by the SCF model. The MTZ model achieved sub-optimal solutions in lower $K\%$ values, whereas the MTZ* model achieved more sub-optimal results in higher $K\%$ values, but both of them were better than the SCF model in these larger regions. In the smaller regions with less than 500 nodes, the MTZ model was better than the MTZ* and SCF models, solving almost all instances in lower $K\%$ values and most instances in higher $K\%$ values to optimality.

We show the average computational times for the MTZ, MTZ* and SCF models and the heuristic method in Table IV. The averages were calculated using only instances where optimality was achieved, and Region-$K\%$ combinations without any optimal solution is shown as '>3600'. From the table, the MTZ model outperforms other MIP models in the relatively larger regions with more than 200 nodes, where as the SCF model outperforms other MIP models in the relatively smaller regions with less than 200 nodes, except for the largest $K\%$ value in rMTL region. When we compare average solution times of the heuristic method (Heur.) and the MIP models, it is clear that the heuristic solution is several magnitudes of order faster than the MIP models. Due to the difficulty in finding optimal solutions for MFC and PCC regions, solution times for the MIP models in these regions are shown as '>3600'. We also investigated the KCT solutions obtained by our heuristic method and compared them with those obtained by the MTZ model when the value of $K\%$ is varied from 10% to 75%. We chose to use the MTZ model as a baseline because it is the overall best MIP model. It was found that overall both MTZ model and heuristic method did not produce different solutions in most cases. In fact, the solutions were mostly identical except the ones in left/right MTL regions with lower two $K\%$ values. This observation is logical because both left/right MTL regions are small, making the KCT problem sizes small. The MTZ model terminated with an optimal solution, and obtained better solutions. All in all, this result confirms that the quality of the heuristic solution is very satisfactory. It should also be noted that there is a large difference in the estimated connectivity between regions. Especially, there is a significant increase in estimated connectivity when more voxels are included, such as in bilateral LPC regions whereas estimated connectivity is quite comparable between the contralateral hemispheres.

B. Discriminating Power

In this section, we investigate which DMN regions played a significant role in separating subject groups into "decliners" and "(stable) non-decliners" as well as compare the sensitivity of our KCT approaches with different values of K. In addition, we also employed the current state-of-the-art regional homogeneity (ReHo) approach to quantify the strength of intra-nodal connectivity of each DMN region [11]. Table V reports the p-values of statistical comparison between decliner vs. non-decliner instances based on connectivity results obtained from KCT and ReHo approaches. The bolded numbers in the table represent p-value < 0.05, and one can observe that the KCT solutions show more discriminating power when $K\%$ is larger, i.e., more voxels are included in the tree. From the

TABLE IV
AVERAGE SOLUTION TIMES (IN SECONDS) FOR DIFFERENT KCT APPROACHES

ROI	K = 10%				K = 25%				K = 50%				K = 75%			
	MTZ	MTZ*	SCF	Heur.	MTZ	MTZ*	SCF	Heur.	MTZ	MTZ*	SCF	Heur.	MTZ	MTZ*	SCF	Heur.
MFC	>3600	>3600	>3600	1.08	>3600	>3600	>3600	1.17	>3600	>3600	>3600	1.70	>3600	>3600	>3600	2.81
PCC	>3600	>3600	>3600	1.56	>3600	>3600	>3600	1.71	>3600	>3600	>3600	1.61	>3600	>3600	>3600	2.31
lLPC	**584**	1233	609	0.53	**634**	2009	958	0.39	**1399**	3096	2059	0.53	1028	>3600	2090	0.84
lMTL	114	126	**22**	0.66	141	216	**31**	0.27	105	748	**47**	0.46	68	1103	**56**	1.01
rLPC	**1240**	2101	1591	0.89	**1705**	2668	3135	0.97	**2447**	>3600	3457	0.80	**2285**	>3600	3541	1.13
rMTL	188	253	**68**	0.69	187	539	**105**	0.80	151	1665	**130**	0.44	**181**	1948	252	0.53

TABLE V
P-VALUES OF STATISTICAL COMPARISON OF THE CONNECTIVITY RESULTS FROM DIFFERENT KCT APPROACHES AND REGIONAL HOMOGENEITY (REHO) BETWEEN DECLINER VS. NON-DECLINER INSTANCES

ROI	K = 10%		K = 25%		K = 50%		K = 75%		K = 100%		ReHo
	Heur.	MTZ	Heur.	MTZ	Heur.	MTZ	Heur.	MTZ	Heur.	MTZ	
MPC	0.9974	N/A	0.7539	N/A	0.5801	N/A	0.4762	N/A	0.4231	N/A	0.7277
PCC	0.2311	N/A	0.5049	N/A	0.8971	N/A	0.8674	N/A	0.7603	N/A	0.7293
lLPC	0.7152	0.6393	0.4929	0.5362	0.4314	0.4148	0.3449	0.3899	0.3994	N/A	0.2904
lMTL	0.1176	0.0898	0.0998	**0.0373**	**0.0363**	**0.0251**	**0.0115**	**0.0106**	**0.0082**	N/A	**0.0333**
rLPC	0.8163	0.9724	0.9201	0.9160	0.7639	0.7493	0.6793	0.6484	0.6180	N/A	0.8332
rMTL	0.3273	0.3412	0.0581	**0.0469**	**0.0253**	**0.0270**	**0.0260**	**0.0217**	**0.0264**	N/A	0.1725

table, the KCT results identified both left and right MTLs as significant regions whereas the ReHo results from the ReHo results was able to detect only the left MTL region. More sensitive results provided by our KCT approaches suggest that both left and right MTLs are the key DMN regions that are significantly altered by cognitive decline and likely to be used as an early biomarker of midlife executive decliners.

VI. CONCLUSION

Accurate early detection of cognitive decline is extremely useful in subjects who start to transition to MCI and are likely to become demented as it will enable early diagnosis and intervention. This can substantially extend a patient's lifespan and some treatments have different outcomes at different disease stages. Recent advanced knowledge about brain function through fMRI studies has allowed researchers and physicians to investigate the DMN, which is functionally active during the resting state, and linked disruptions in DMN connectivity with many brain disorders ranging from Alzheimer's disease (AD), to autism spectrum disorder (ASD), to Parkinson's disease (PD). However, previous DMN studies are mostly focused on large-scale connectivity between DMN regions, disregarding patterns of local connectivity. The overall goal of this study is to develop a network optimization framework as a computational tool to identify underlying, critical structures in local connectivity within individual DMN regions. As propagation pathway (tree-like) is believed to be the critical connectivity structure within DMN regions, this paper presents a model of critical connectivity within DMN regions as a KCT problem. This model is supported by several previous investigations, which conclude that the exact location and size of the brain regions that are involved in the DMN are not known. Thus one needs to investigate local connectivity of different sizes (varying the value of $K\%$ in our case).

To solve the KCT problem, we introduced a novel compact MIP formulation based on single commodity flow (SCF) model and improved a formulation based on Miller-Tucker-Zemlin (MTZ) constraints by introducing node selector variables. These two models allowed KCT problem to be conveniently solved using commercial solvers. We incorporated symmetry breaking constraints, which are typically found in branch-and-cut models for KCT, into our formulations to enhance their performance. We also introduced a heuristic method based on Kruskal's algorithm for minimum spanning trees. We conducted comparative computational experiments on brain regions using our formulations and other compact formulations in the literature. We showed that our SCF formulation was effective in smaller instances and MTZ formulation handled large problems well, while other formulations could not even achieve optimality in any problem. We also provided LP relaxation bounds for our two formulations to explain their behavior in regards to different problem sizes. Some brain regions were too large for any formulation to achieve optimality due to the fact that KCT is a NP-hard problem. However, our heuristic method, which produced high-quality results to optimal solutions in small and medium size problems, scaled very well for the large instances with a running time several magnitudes of order faster than the MIP models.

Identification of local connectivity strengths and configurations could provide a noninvasive biomarker for brain health, and aid in the assessment of neuroprotective strategies. The computational methods presented in this paper can be considered as a necessary first step to develop useful tools for system neuroimaging that can be employed and tested a novel biomarker of cognitive decline for those who are at risk of developing MCI and AD. These tools will also enable the methodical uncovering of abnormal alterations in brain function and bring fresh insight into mechanisms of brain diseases. This will eventually lead to targeted therapeutics, including cognitive enhancers and protective brain agents, identify transition stages between normal brain aging to cognitive impairment and perhaps evaluate functional networks of cognitive phenotypes associated with MCI and AD.

REFERENCES

[1] S. M. Hofer and D. F. Alwin, Eds., *Handbook of Cognitive Aging: Interdisciplinary Perspectives*. Los Angeles, CA, USA: Sage, 2008.
[2] R. C. Petersen, "Mild cognitive impairment," *New England J. Med.*, vol. 364, pp. 2227–2234, Jun. 2011.

[3] S. M. Smith *et al.*, "Correspondence of the brain's functional architecture during activation and rest," *Proc. Nat. Acad. Sci. USA*, vol. 106, no. 31, pp. 13040–13045, 2009.
[4] J. S. Damoiseaux *et al.*, "Reduced resting-state brain activity in the 'default network' in normal aging," *Cerebal Cortex*, vol. 18, no. 8, pp. 1856–1864, 2007.
[5] W. W. Seeley *et al.*, "Dissociable intrinsic connectivity networks for salience processing and executive control," *J. Neurosci., Official J. Soc. Neurosci.*, vol. 27, no. 9, pp. 2349–2356, 2007.
[6] M. Pievani, W. de Haan, T. Wu, W. W. Seeley, and G. B. Frisoni, "Functional network disruption in the degenerative dementias," *Lancet Neurol.*, vol. 10, no. 9, pp. 829–843, 2011.
[7] S. J. Broyd, C. Demanuele, S. Debener, S. K. Helps, C. J. James, and E. J. S. Sonuga-Barke, "Default-mode brain dysfunction in mental disorders: A systematic review," *Neurosci. Biobehavioral Rev.*, vol. 33, no. 3, pp. 279–296, Mar. 2009.
[8] N. J. Minshew and T. A. Keller, "The nature of brain dysfunction in autism: Functional brain imaging studies," *Current Opinion Neurol.*, vol. 23, no. 2, pp. 124–130, 2010.
[9] I. M. Veer *et al.*, "Whole brain resting-state analysis reveals decreased functional connectivity in major depression," *Frontiers Syst. Neurosci.*, vol. 4, p. 41, Sep. 2010.
[10] K. Çiftçi, "Minimum spanning tree reflects the alterations of the default mode network during alzheimer's disease," *Ann. Biomed. Eng.*, vol. 39, no. 5, pp. 1493–1504, 2011.
[11] Y. Zang, T. Jiang, Y. Lu, Y. He, and L. Tian, "Regional homogeneity approach to fMRI data analysis," *NeuroImage*, vol. 22, no. 1, pp. 394–400, 2004.
[12] A. F. Alexander-Bloch *et al.*, "Disrupted modularity and local connectivity of brain functional networks in childhood-onset schizophrenia," *Frontiers Syst. Neurosci.*, vol. 4, p. 147, Oct. 2010.
[13] J. Sepulcre, H. Liu, T. Talukdar, I. Martincorena, B. T. T. Yeo, and R. L. Buckner, "The organization of local and distant functional connectivity in the human brain," *PLoS Comput. Biol.*, vol. 6, no. 6, p. e1000808, 2010.
[14] D. S. Margulies *et al.*, "Resting developments: A review of fMRI post-processing methodologies for spontaneous brain activity," *Magn. Reson. Mater. Phys., Biol. Med.*, vol. 23, nos. 5–6, pp. 289–307, 2010.
[15] C. Habeck and J. R. Moeller, "Intrinsic functional-connectivity networks for diagnosis: Just beautiful pictures?" *Brain Connectivity*, vol. 1, no. 2, pp. 99–103, Aug. 2011.
[16] Y. I. Sheline and M. E. Raichle, "Resting state functional connectivity in preclinical Alzheimer's disease," *Biol. Psychiatry*, vol. 74, no. 5, pp. 340–347, 2013.
[17] M. Greicius, "Resting-state functional connectivity in neuropsychiatric disorders," *Current Opinion Neurol.*, vol. 21, no. 4, pp. 424–430, 2008.
[18] J. R. Andrews-Hanna *et al.*, "Disruption of large-scale brain systems in advanced aging," *Neuron*, vol. 56, no. 5, pp. 924–935, 2007.
[19] S. Achard and E. Bullmore, "Efficiency and cost of economical brain functional networks," *PLoS Comput. Biol.*, vol. 3, no. 2, p. e17, 2007.
[20] D. Meunier, R. Lambiotte, and E. T. Bullmore, "Modular and hierarchically modular organization of brain networks," *Frontiers Neurosci.*, vol. 4, p. 200, Dec. 2010.
[21] X. Wang, R. Hutchinson, and T. M. Mitchell, "Training fMRI classifiers to discriminate cognitive states across multiple subjects," in *Proc. NIPS*, vol. 16. 2003, pp. 709–716.
[22] J.-T. Wu *et al.*, "Aging-related changes in the default mode network and its anti-correlated networks: A resting-state fMRI study," *Neurosci. Lett.*, vol. 504, no. 1, pp. 62–67, Oct. 2011.
[23] M. Fischetti, H. W. Hamacher, K. Jørnsten, and F. Maffioli, "Weighted k-cardinality trees: Complexity and polyhedral structure," *Networks*, vol. 24, no. 1, pp. 11–21, 1994.
[24] M. Ehrgott and J. Freitag, "K_TREE/K_SUBGRAPH: A program package for minimal weighted K-cardinlity trees and subgraphs," *Eur. J. Oper. Res.*, vol. 1, no. 93, pp. 214–225, 1996.
[25] M. Ehrgott, J. Freitag, H. W. Hamacher, and F. Maffioli, "Heuristics for the K-cardinality tree and subgraph problems," *Asia–Pacific J. Oper. Res.*, vol. 14, no. 1, pp. 87–114, 1997.
[26] M. J. Blesa and F. Xhafa, "A C++ implementation of tabu search for k-cardinality tree problem based on generic programming and component reuse," in *Proc. GCSE Young Res. Workshop*, 2000, pp. 1–13.
[27] M. J. Blesa, P. Moscato, and F. Xhafa, "A memetic algorithm for the minimum weighted k-cardinality tree subgraph problem," in *Proc. 4th Metaheuristics Int. Conf. (MIC)*, vol. 1. Porto, Portugal, 2001, pp. 85–90.
[28] N. Mladenović and D. Urošević, "Variable neighborhood search for the k-cardinality tree," in *Metaheuristics: Computer Decision-Making*. Norwell, MA, USA: Kluwer, 2004, pp. 481–500.
[29] C. Blum and M. J. Blesa, "New metaheuristic approaches for the edge-weighted k-cardinality tree problem," *Comput. Oper. Res.*, vol. 32, no. 6, pp. 1355–1377, 2005.
[30] S. Arora and G. Karakostas, "A $(2+\epsilon)$-approximation algorithm for the k-MST problem," in *Proc. 11th Annu. ACM-SIAM Symp. Discrete Algorithms (SODA)*, 2000, pp. 754–759.
[31] A. Blum, R. Ravi, and S. Vempala, "A constant-factor approximation algorithm for the k-MST problem," in *Proc. ACM Symp. Theory Comput.*, 1996, pp. 442–448.
[32] N. Garg, "A 3-approximation for the minimum tree spanning k vertices," in *Proc. 37th Annu. Symp. Found. Comput. Sci. (FOCS)*, 1996, pp. 302–309.
[33] N. Garg, "Saving an epsilon: A 2-approximation for the k-MST problem in graphs," in *Proc. 27th Annu. ACM Symp. Theory Comput. (STOC)*, 2005, pp. 396–402.
[34] M. X. Goemans and D. P. Williamson, "A general approximation technique for constrained forest problems," *SIAM J. Comput.*, vol. 24, no. 2, pp. 296–317, 1995.
[35] F. P. Quintão, A. S. da Cunha, G. R. Mateus, and A. Lucena, "The k-cardinality tree problem: Reformulations and Lagrangian relaxation," *Discrete Appl. Math.*, vol. 158, no. 12, pp. 1305–1314, 2010.
[36] M. Chimani, M. Kandyba, I. Ljubić, and P. Mutzel, "Obtaining optimal k-cardinality trees fast," *J. Experim. Algorithmics*, vol. 14, pp. 5:2.5–5:2.23, Dec. 2009.
[37] L. Simonetti, F. Protti, Y. Frota, and C. C. de Souza, "New branch-and-bound algorithms for k-cardinality tree problems," *Electron. Notes Discrete Math.*, vol. 37, pp. 27–32, Aug. 2011.
[38] L. Simonetti, A. S. da Cunha, and A. Lucena, "Polyhedral results and a branch-and-cut algorithm for the k-cardinality tree problem," *Math. Program.*, vol. 142, nos. 1–2, pp. 511–538, 2013.
[39] K. W. Schaie, *Developmental Influences on Adult Intelligence: The Seattle Longitudinal Study*. Oxford, U.K.: Oxford Univ. Press, 2005.
[40] D. Meunier, S. Achard, A. Morcom, and E. Bullmore, "Age-related changes in modular organization of human brain functional networks," *NeuroImage*, vol. 44, no. 3, pp. 715–723, 2009.
[41] C. F. Beckmann and S. M. Smith, "Probabilistic independent component analysis for functional magnetic resonance imaging," *IEEE Trans. Med. Imag.*, vol. 23, no. 2, pp. 137–152, Feb. 2004.
[42] N. Filippini *et al.*, "Distinct patterns of brain activity in young carriers of the *APOE*-ε4 allele," *Proc. Nat. Acad. Sci. USA*, vol. 106, no. 17, pp. 7209–7214, Apr. 2009.
[43] C. E. Miller, A. W. Tucker, and R. A. Zemlin, "Integer programming formulation of traveling salesman problems," *J. Assoc. Comput.*, vol. 7, no. 4, pp. 326–329, 1960.
[44] M. Desrochers and G. Laporte, "Improvements and extensions to the Miller–Tucker–Zemlin subtour elimination constraints," *Oper. Res. Lett.*, vol. 10, no. 1, pp. 27–36, 1991.

AQ:3

AQ:4

W. Art Chaovalitwongse, photograph and biography not available at the time of publication.

Daehan Won, photograph and biography not available at the time of publication.

Onur Seref, photograph and biography not available at the time of publication.

Paul Borghesani, photograph and biography not available at the time of publication.

M. Katie Askren, photograph and biography not available at the time of publication.

Sherry Willis, photograph and biography not available at the time of publication.

Thomas J. Grabowski, photograph and biography not available at the time of publication.

AUTHOR QUERIES

AUTHOR PLEASE ANSWER ALL QUERIES

PLEASE NOTE: We cannot accept new source files as corrections for your paper. If possible, please annotate the PDF proof we have sent you with your corrections and upload it via the Author Gateway. Alternatively, you may send us your corrections in list format. You may also upload revised graphics via the Author Gateway.

AQ:1 = Please confirm whether the edits made in the financial section are OK.
AQ:2 = Please confirm whether the edits made in the current affiliation of all the authors are OK as set.
AQ:3 = Please confirm that ref. [26] is correct as set.
AQ:4 = Please provide authors' biographies.